SAR-BASED OBSERVATIONS AND FAULT SOURCE MODELING OF THE CO-SEISMIC DEFORMATION: THE 2008 ZHONGBA EARTHQUAKE (M6.7) AND THE 2010/2011 SE IRAN EARTHQUAKES (M6.5 and M6.2)

Space Geodesy, Earth and Planetary Dynamics

Department of Natural History Sciences,

Graduate School of Science, Hokkaido University

Shuoshuai Sun

Abstract

In this paper, we used spaceborne SAR data to get InSAR figures and using those data to make the three-dimensional fault source models. This time, we did the research on two recent earthquakes. First one is the Aug. 25th, 2008 Zhongba earthquake which happened in South Tibet, China, and the magnitude given by Global Centroid Moment Tensor (GCMT) is 6.7. The other is the Dec. 20th, 2010 earthquake happened in South-eastern Iran whose moment magnitude given by GCMT is 6.5.

We used both the ALOS data and ESA data for the Zhongba earthquake which happened on 25th Aug. 2008, and using the two independent interferograms. We inverted the three dimensions model and also get the distribution. The strike slip and dip slip from our model are 1.2m and 0.9m, respectively.

While for the 20th Dec. 2010 earthquake, we only used the ALOS data. Beside the strimp-mode SAR data, the ScanSAR data also been used. In addition, the Pixel offset data also been used this time, which is useful to get displacement in north and south direction. We also make the three-dimensional fault model inverted from the three Interferograms, and get the slip distribution. This time, there are mainly happened with strike slip which is around 2.5m and almost no dip slip. One month later after the Dec. earthquake, another aftershock happened on Jan. 27th, 2011 which is worth to focus on due to its moment magnitude and the near location of the Dec. earthquake. So we made the interferograms used both ALOS and Envisat data and inverted the three-dimensional fault source again hope we can find some connection. The Jan. earthquake also happened mainly with strike slip around 0.9m, but this time a little dip slip happened. Consider both of the two recent SE Iran earthquakes, the location of our two models shows that they occurred on different fault plane instead of a single one.

From our best-fitting fault source model, each calculated moment magnitude is in a good agreement with GCMT. While the Depth is about 10km shallower than the information given by GCMT, and the location is also about 10km away from the location given by GCMT.

Key words: InSAR; Fault Source Model; Strike Slip; Dip Slip

Contents

1. Introduction

1.1 Space Geodetic Techniques for Crustal Deformation

Crustal deformation data have been traditionally acquired by ground-based geodetic techniques such as leveling, triangulation, and electro-optic distance measurement. More recently, global positioning system (GPS) has become a standard tool for high-precision crustal deformation measurement, and provided us with a wealth of data to study plate tectonics, earthquakes, volcanic activities, and atmospheric and hydrological loading deformation. All these techniques, however, require in-situ benchmarks, and thus prevent us from observing inaccessible areas. Interferometric SAR (InSAR) was, therefore, regarded as a surprising and revolutionary technique when Massonnet et al. (1993) first showed an image of the co-seismic deformation associated with the 1992 M7.3 Landers earthquake, because the raw data was completely acquired on a spaceborne sensor. Another big surprise for the community was its incredibly high spatial resolution, which no other geodetic techniques were possible to achieve in practice.

1.2 Background of Tibet and Iran
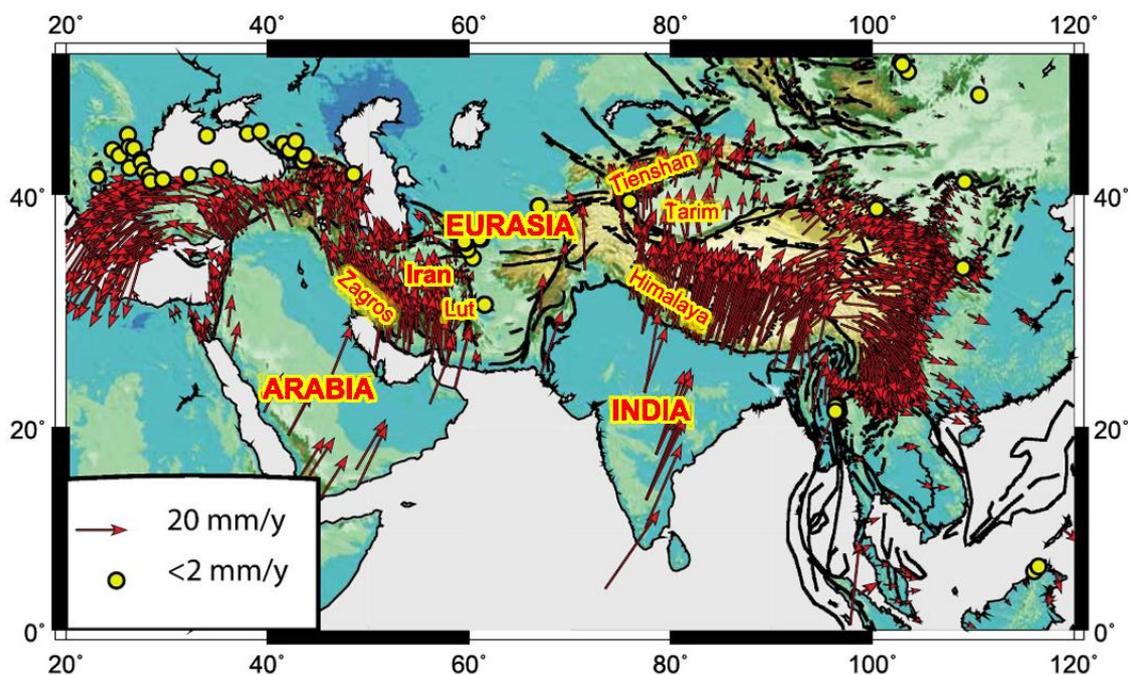
Figure 1.1 Plate tectonics around Tibet and Iran by GPS

The Arabian Plate and Indian Plate moving north to the Eurasia Plate, and the collision are about 25 mm/y given by Denis Hatzfeld and Peter Molnar (2010). Tibet

and Iran are located in the boundary of the three plates, so that the earthquake often happened in those areas.
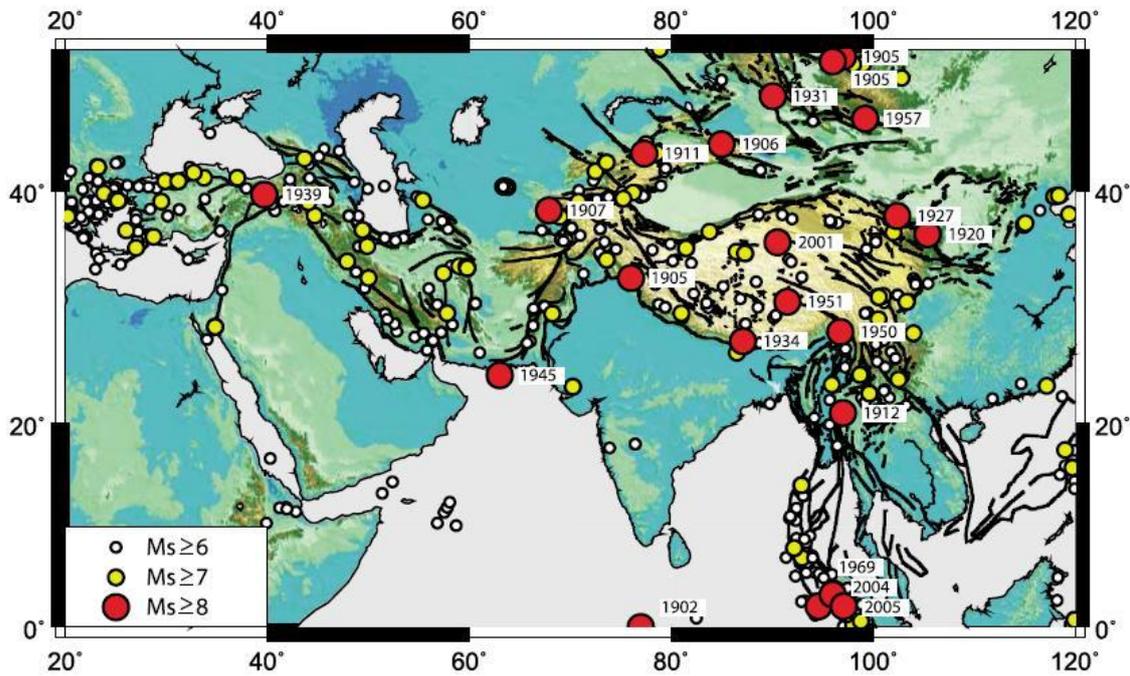

Figure 1.2 Earthquakes happened between1900~2005

Although earthquakes with magnitude 6+ often happen in those areas, there are no large earthquakes happened before.

1.3 Motivation

Both Tibet and Iran are very few GPS-based on-going crustal deformation data. Also due to the high altitude of Tibet, and less resident in SE Iran, SAR data can give a significant help.

We make the three-dimensional fault source model from geodetic data, and compare it to the model from seismology. Since the seismology data can only give the inaccurate epicentre locations and the centroid moment tensor is at a point, SAR data can be used to solve these issues. Finally, this kind of work can make any contribution to the understanding of the regional active tectonics.

2. Methods

2.1 InSAR technology

2.1.1 SAR Data

SAR is acronym for Synthetic Aperture Radar. A technique to image any ground surfaces, using airborne or spaceborne radar sensor. Its high spatial resolution is achieved by collecting numerous return pulses from each target in sight and by effectively synthesizing large antenna size.

InSAR is acronym of Interferometric SAR and is a powerful technique to image surface topography and ground displacements, using phase values of two or more SAR images.
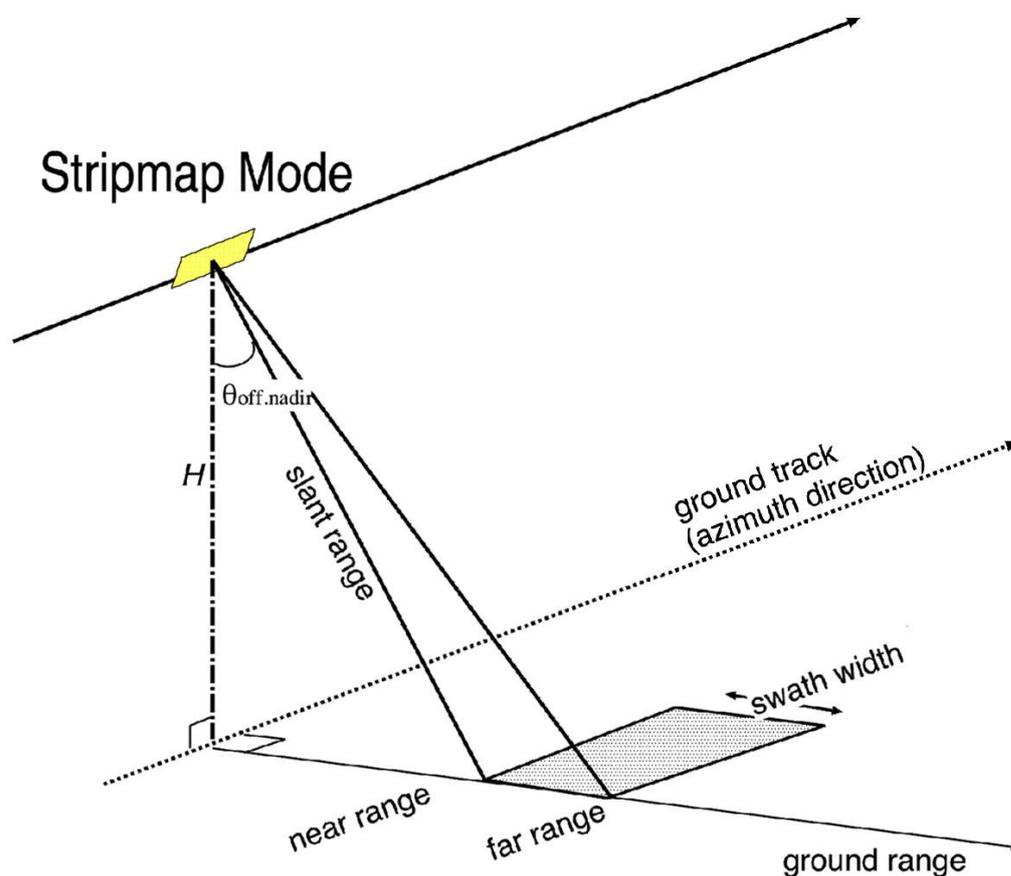
Figure 2.1 stripmap mode

SAR satellite flies over at an altitude of hundreds of km, repeating transmission and reception of microwave pulses. The along-track and across-track axes are almost identical to the azimuth and range axis in the acquired radar image. The area illuminated on the ground is called swath, whose width spans roughly 50-100 km in the standard stripmap (or strip) mode with an incidence angle of 20-50 degrees (Figure 2.1). While

previous SAR applications are mostly derived from the stripmap mode, another imaging mode, ScanSAR, is also promising, because it covers much wider swath width, 300-500 km, by illuminating multiple swaths at the expense of reducing the resolution (figure 2.2).
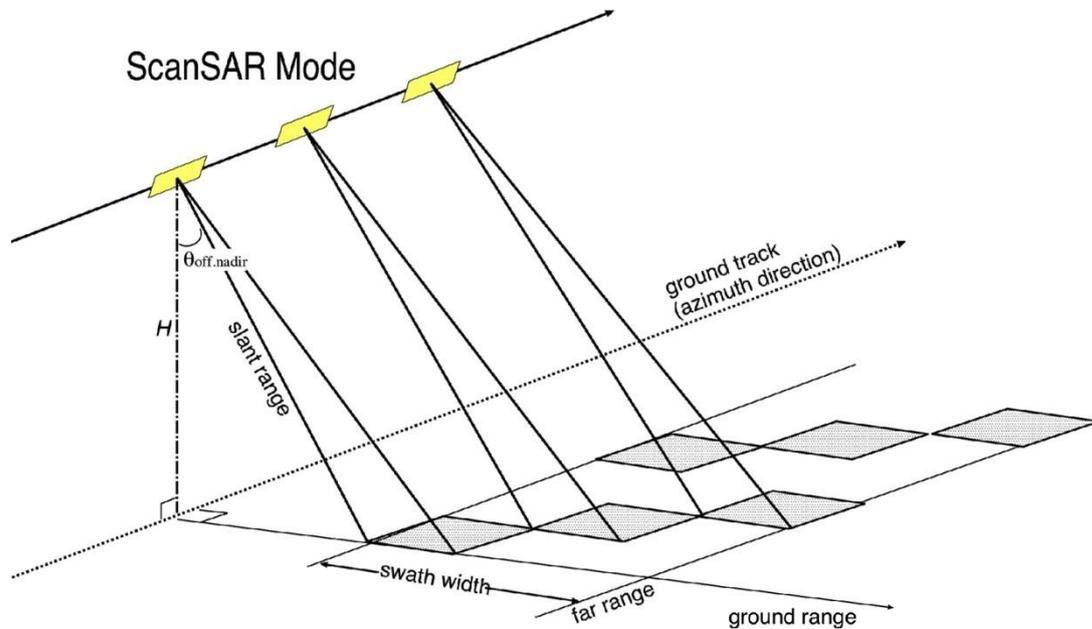

Figure 2.2 ScanSAR mode

2.1.2 ALOS and Envisat

2.1.2.1 ALOS

Figure 2.3 ALOS

Advanced Land Observing Satellite (ALOS), also called Daichi, is a 4-ton Japanese satellite which was launched from Tanegashima Island, Japan on 24 January 2006 by an H-IIA rocket. ALOS followed the Japanese Earth Resources Satellite-1 (JERS-1) and Advanced Earth Observing Satellite (ADEOS) and utilized advanced land-observing

technology. ALOS was used for cartography, regional observation, disaster monitoring, and resource surveying. The ALOS has three remote-sensing instruments: the Panchromatic Remote-sensing Instrument for Stereo Mapping (PRISM) for digital elevation mapping, the Advanced Visible and Near Infrared Radiometer type 2 (AVNIR-2) for precise land coverage observation, and the Phased Array type L-band Synthetic Aperture Radar (PALSAR) for day-and-night and all-weather land observation. In order to utilize fully the data obtained by these sensors, the ALOS was designed with two advanced technologies: the former is the high speed and large capacity mission data handling technology, while the latter is the precision spacecraft position and attitude determination capability. They will be essential to high-resolution remote sensing satellites in the next decade.

The Phased Array type L-band Synthetic Aperture Radar (PALSAR) is an active microwave sensor using L-band frequency to achieve cloud-free and day-and-night land observation, which we used in our research. It provides higher performance than theJERS-1's synthetic aperture radar (SAR). Fine resolution in a conventional mode, but PALSAR will have another advantageous observation mode. ScanSAR, which will enable us to acquire a 250 to 350km width of SAR images (depending on the number of scans) at the expense of spatial resolution. This swath is three to five times wider than conventional SAR images. Our later part we expatiate on the ScanSAR in detail since we used this in when we did the research about Iran.

2.1.2.2 Envisat

Figure 2.4 Envisat

Envisat which was launched by European Space Agency (ESA) on 1st March, 2002

was the successor to two European Remote Sensing (ERS) satellites.

More advanced imaging radar, radar altimeter and temperature-measuring radiometer instruments extend ERS data sets. This is supplemented by new instruments including a medium-resolution spectrometer sensitive to both land features and ocean color. Envisat also carries two atmospheric sensors monitoring trace gases.

The latest news for Envisat was, ESA announced that they lost the contact with Envisat since 12th April, 2012. ESA formally announced the end of Envisat's Mission on 9th May, 2012.

We can do nothing to retrieve anything, just thanks to the work ALOS and Envisat done. We sincerely wait for the next generation of SAR satellite to launch.

2.1.3 The Difference of GPS and InSAR

As we know that both Global Positioning System (GPS) and SAR are very useful to detective the crustal movement of the earth, and they have their own characteristics. Here we will give a compare of the two technologies and then mainly interpret SAR technology.

Table 2.1 The comparison of GPS and InSAR.

	GPS	InSAR
Observation Facilities	Receiver Required	Unnecessary
2-dimensional Information	Impossible	Possible
Direction of Measurement	3-Dimensional	1-Dimensional (LOS)
Observation Time	24 hours available	Once every dozens of days

2.2 Pixel Offset

Before we get an initial interferogram, we must register (or, match) each imaged target in one SLC image to the same target in the other SLC image with a sub-pixel level accuracy, because any ground objects do not usually locate at the same pixel coordinates in each SLC image. This pre-processing is called image registration (or image matching) and prerequisite to be performed prior to generating an initial interferogram. Although a simple polynomial transformation between the range and azimuth coordinates of two SLC images is sufficient in most cases, we need to take into account the effects of 3-D topography when the terrain surface is rugged to eliminate a

stereoscopic effect (Michel et al., 1999).
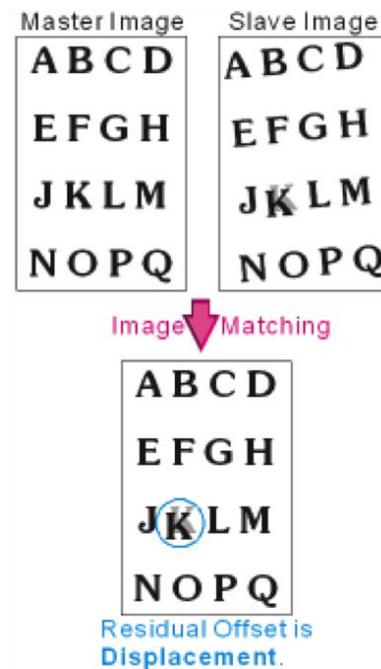
Figure 2.5 Pixel Offset

When large ground displacements on the order of meters or more take place locally, and if we correct for the long-wavelength image distortion using the polynomial transformation, we can detect and quantify those localized displacements as a by-product of image registration without viewing InSAR image (Tobita et al., 2001a). This approach to detect large displacements is called pixel offset or feature tracking technique, and has been applied to earthquakes, volcanic eruptions, and glacier movements. The advantages of pixel offset data are two folds. First, pixel offset data can quantify large displacements even in such areas that completely loses interferometric coherence, where InSAR data cannot be unwrapped; we describe coherence and unwrapping later below. Secondly, in contrast to InSAR data, pixel offset data provide us with not only range offset but also azimuth offset component. While the range offset has the same sensitivity to the 3-D displacement vector as InSAR data, the azimuth offset is a projection of the displacement vector onto the unitary vector perpendicular to the LOS. Hence, the azimuth offset data are complementary to the range offset or InSAR data. Taking advantage of this property, Fialko et al. (2001) derived a full 3-D displacement map for the 1999 M7.1 Hector Mine earthquake, combining the InSAR data from both ascending and descending track with the azimuth

offset data. Using pixel offset data from both descending and ascending track, Tobita et al. (2001a, b) inferred a 3-D displacement map associated with the 2000 eruption episode at Usu volcano.

2.3 Interferometric SAR Procedure

We process the SAR data to get interferogram and from which we can know the deformation caused by earthquake. From the image registration, flattening, phase unwrapping, to the geocoding, we can get the interferogram in a ground-based coordinate and using which to know the crustal deformation caused by earthquake.
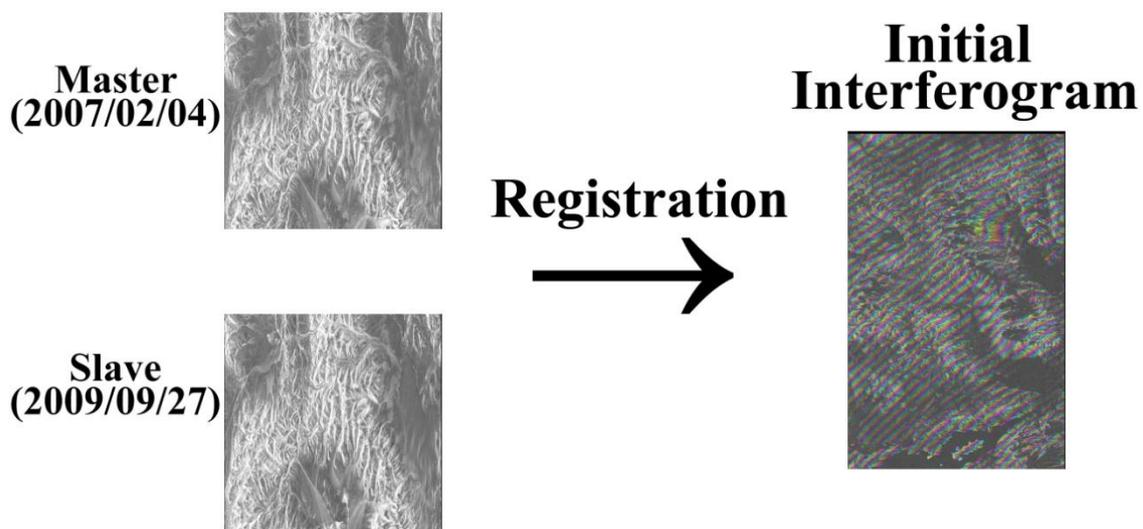
Figure 2.6 image registration

Image registration (Matching): Before we get an initial interferogram, we must register (or, match) each imaged target in one SLC image to the same target in the other SLC image with a sub-pixel level accuracy, because any ground objects do not usually locate at the same pixel coordinates in each SLC image. This pre-processing is called image registration (or image matching) and prerequisite to be performed prior to generating an initial interferogram.

Flattening: The observed data contains three parts of fringes, the first is the orbit fringes, and the second is the topography fringes, and the third is deformation fringes. Of course, not all the fringes are needed, so we simulate a data from Digital Elevation Model (DEM) and orbit data. We subtract the simulated data to the observed data, so we can only get the deformation data which is we really needed.
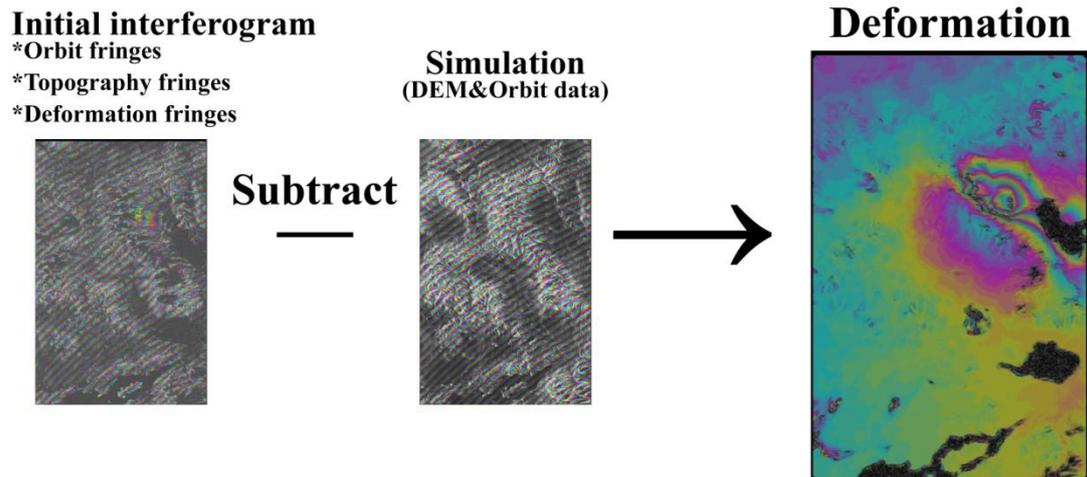
Figure 2.7 Flattening
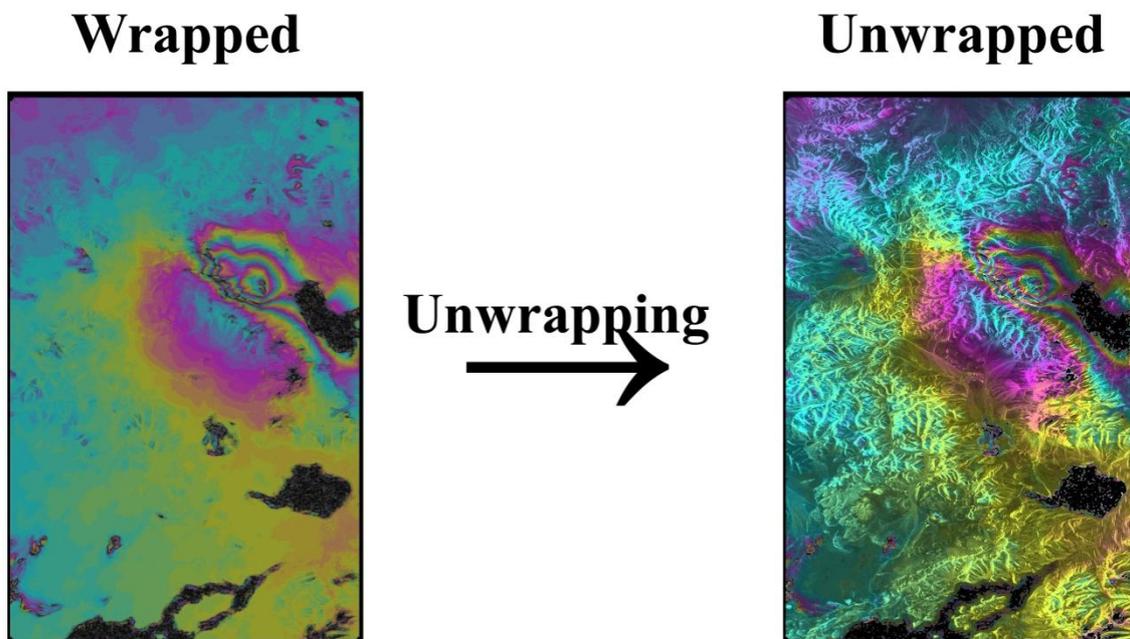
Figure 2.8 Phase Unwrapping

Phase Unwrapping: the results of InSAR analysis are mostly shown as pictures with colored fringes. What is actually measured by SAR is the phase of the wave and not the absolute distance. The phase is represented by an angle from 0 to 360 degrees, and after one cycle, it returns to 0 degree. A color in interference fringe pattern of the interferogram shows the difference in phases caused by the difference in distance between observations of that point.

A phase difference of 360 degrees means that the distance that a radio wave travels back and forth between a radar and the ground changes by just one wavelength.

As such, the phase difference of a radio wave is proportional to the displacement, and the color of the fringe pattern shows the magnitude of deformation at that point.

However, the phase returns to zero after it reaches 360 degrees. This means that the displacement corresponding to the integral multiples of 360 degrees has the same phase. Responding to the indefiniteness in the phase difference of 360 degrees, the surface deformation obtained by InSAR also includes indefiniteness in the integral multiples of (the wavelength of radar wave)/2. This means that when a color at a certain point on the SAR interferogram of ALOS indicates a displacement corresponding to 5 centimeters, the actual displacement may be $5 \pm 11.8 \times n$ (n is a integer, 0, 1, 2 …).

In order to resolve such indefiniteness, the following procedure is used. When the color change in the SAR interferogram starts from the point where the surface deformation is zero and ends in the point where the same color change is repeated after completing one cycle, it can be said that the latter point has the phase difference of 360 degrees, i.e., the displacement of 11.8 centimeters. Where the color change is repeated in 2 complete cycles, the displacement is double, 23.6 centimeters.

A technique to combine such a sequence is called as "Phase Unwrapping." With this technique, the absolute amount of actual surface deformation can be determined.
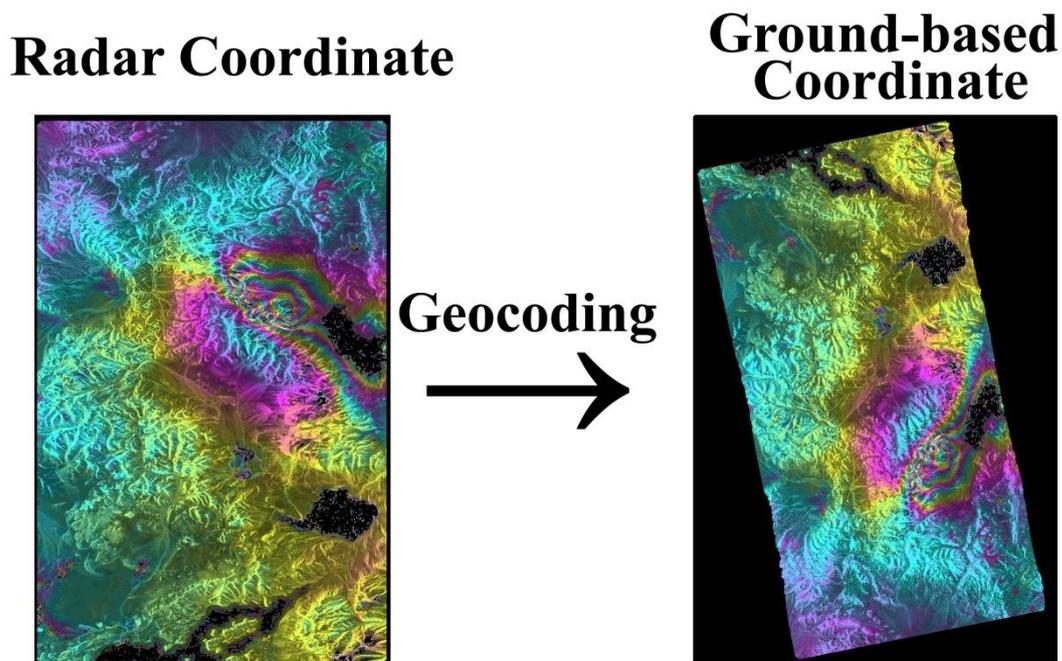

Figure 2.9 Geocoding

Geocoding: In the analysis of InSAR, the data are processed in the radar coordinate

system obtained by the SAR satellite, and the results are converted to the ground-based coordinate system by using elevation data. This process is called "Geocoding." In this process, pixels holding information are rearranged according to longitude and latitude. So, the projection method employed in the SAR interferogram is the equidistant cylindrical projection or the equirectangular projection.

Thus, we can get the interferogram using the procedure are shown above, and after we get more than two independent data, we can make the three-dimensional fault source model to better understand the slip distribution under the ground.

2.4 Modeling

Fault source model is such a model that can reasonably reproduce the observed data, and the model is specified with its geometry and slip distribution. This time, we also use the 2008 Zhongba earthquake to show how we make the model.

Before we make the model, we should reduce the number of observed data employ the quad tree decomposition, which can reduce the number of data without losing any important information. This works like the
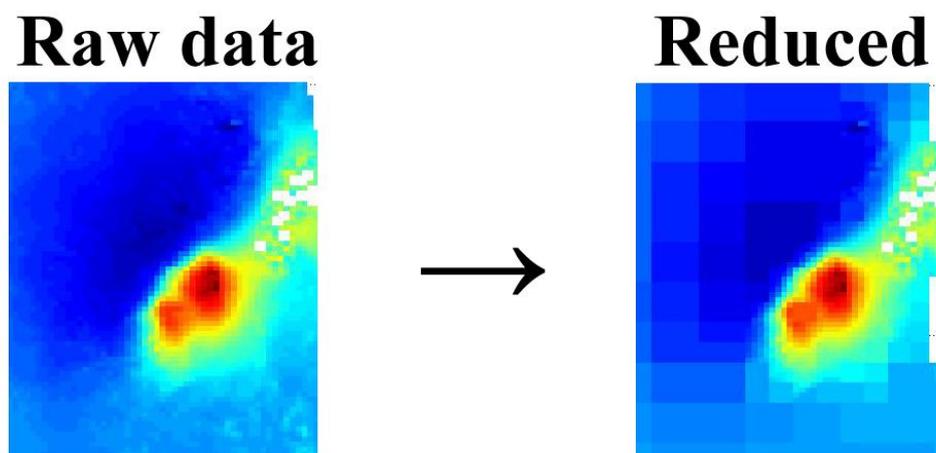

Figure 2.10 Quad-tree Decomposition

After we get the smaller data, we will make the preliminary location of the fault. We make the geometry by Gmsh, and the upper of the geometry is made visually from the observed data, and put the model along the boundary. The part underground just make freely at the beginning.

After we made the geometry, we will employ the green function due to triangular dislocation element, and then impose non-negativity constraint on the slip direction and

impose smoothness constraint on the slip distribution.
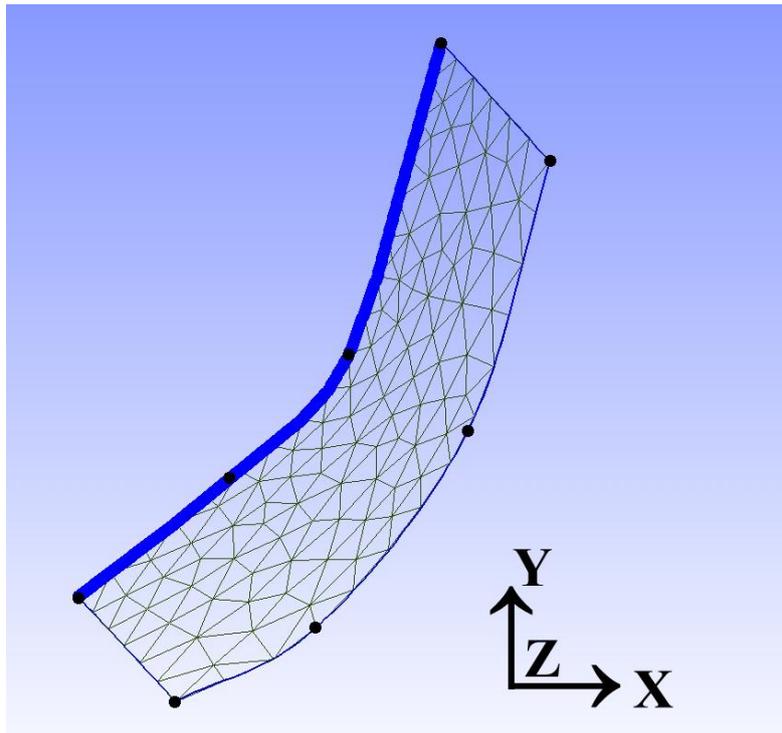

Figure 2.11 Preliminary Location

Compared the residual which subtracted between the observed data and calculated data, we will change the geometry until we find the best-fitting model. For all the procedure, we name it trial and error.

In the later chapters, we will show the results made from InSAR and the fault source modelling.

3. Results (Observation and Modelling)

3.1 August 25th 2008, Zhongba County, Tibet, China (Mw6.7)

3.1.1 Background

An earthquake with magnitude 6.7 struck Zhongba County, western Tibet, China, on 25th August 2008, whose focal mechanism was normal faulting according to the GCMT project. Although normal faulting earthquake often takes place in Tibetan plateau, it remains uncertain why normal faulting earthquakes present in the present Tibetan plateau despite the on-going northward compression associated with the Indian plate motion. We use InSAR observations to estimate the fault slip distribution of the Zhongba Earthquake, and infer the fault source model so that we will be able to gain any insights into the origin of normal faulting earthquakes.

3.1.2 Observed area and Dataset
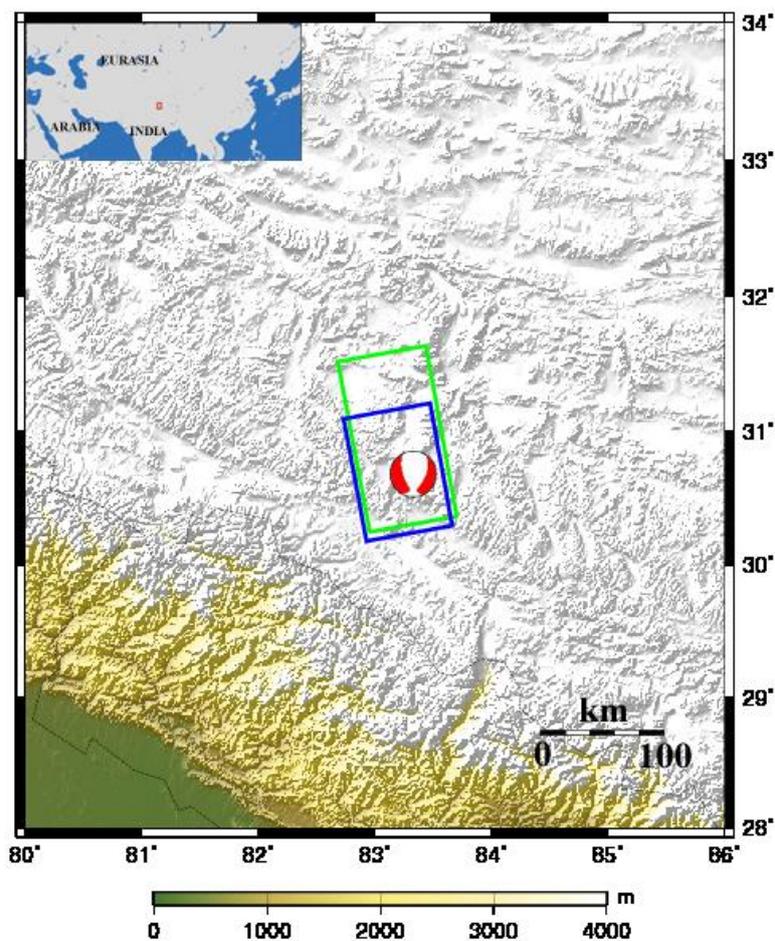
Figure 3.1 The district of this earthquake and the region for our observation data. The green rectangular stands for the observed area by ALOS and the blue one stands for the observed area from Envisat.

We used many pairs in order to get a better interferogram, Table 1 give the data we used. We only show the best interferogram from ALOS whose master is 2007/02/04 and slave is 2009/09/27.

Table 3.1 The data we used and the basic information of the data.

Pair No.	Master (yyyy/mm/dd)	Slave (yyyy/mm/dd)	Bperp* (m)	Span (days)	Orbit	Satellite
1	2007/02/04	2009/06/27	-213	874	Ascending	ALOS
2	2007/02/04	2009/09/27	27	966	Ascending	ALOS
3	2007/08/07	2009/12/28	-183	874	Ascending	ALOS
4	2008/02/07	2010/08/15	-35	900	Ascending	ALOS
5	2008/05/09	2010/08/15	-596	828	Ascending	ALOS
6	2008/08/21	2008/10/30	-142	70	Ascending	Envisat

* Bperp represents for Perpendicular baseline.

3.1.3 Interference Pattern
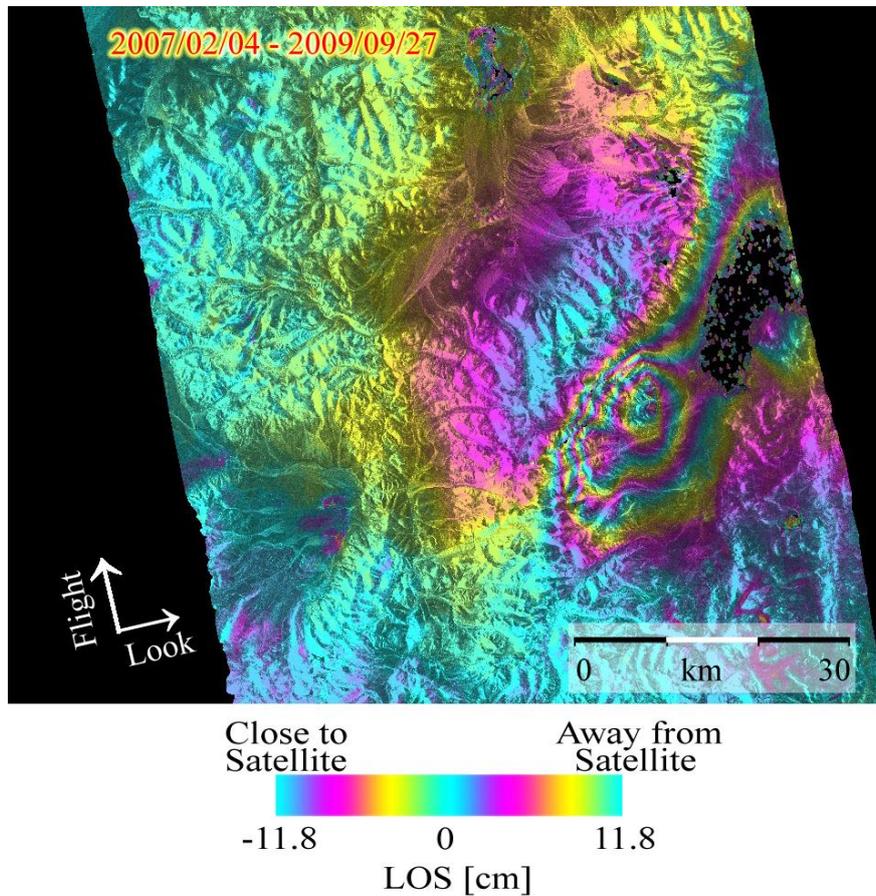
Figure 3.2 the results of InSAR figures from ALOS/PALSAR.
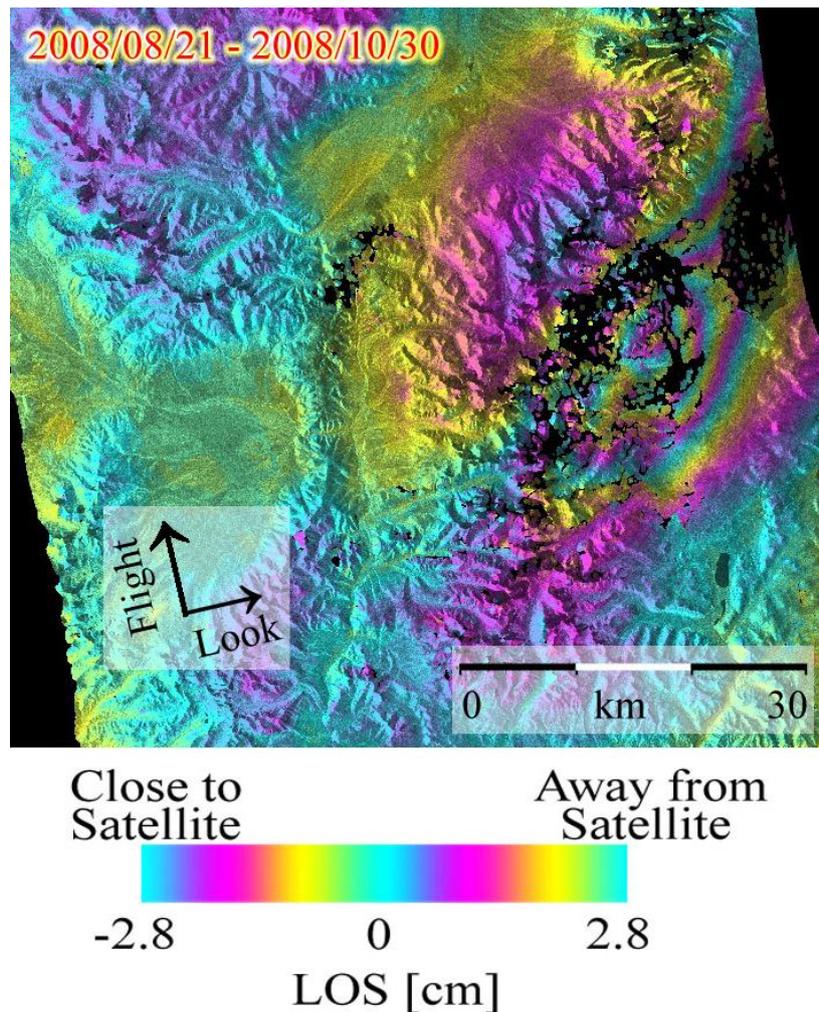
Figure 3.3 the results of InSAR figures from Envisat/ASAR.

We used both ALOS and Envisat data to detect the signal of this earthquake by InSAR technology, and clear interference pattern can be seen from both of them. For ALOS data, the master and slave image spanned two year include the date when this earthquake happened, while the Evisat data only spanned two month include the earthquake happened date.

3.1.4 Inversion result

We this time processed the InSAR data made by both ALOS and Envisat in order to invert the slip distribution. We made the three dimension model by Gmsh to detect the fault rupture, while comparing the calculated data to the observed data by using Matlab, we could estimate whether our model is good enough or not. We changed the model and compare the residual error again and again, and this kind of work has done until the calculated data looks similar to the observed data. After doing all of these we could get the Strike Slip and Dip Slip of the earthquake in three-dimensions. Figure 3.4 below

gives the result and from which we can see the calculated data looks similar to the observed data, and the residual is less than 10 cm.
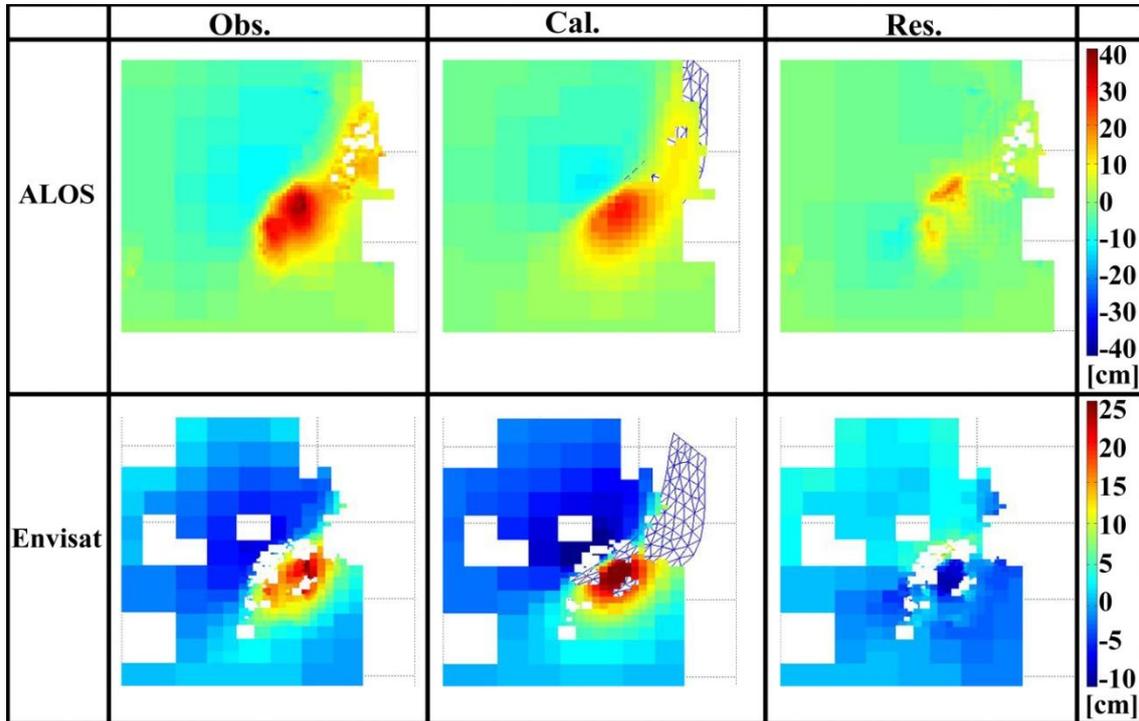

Figure 3.4 the inversion result using only two independent InSAR data.
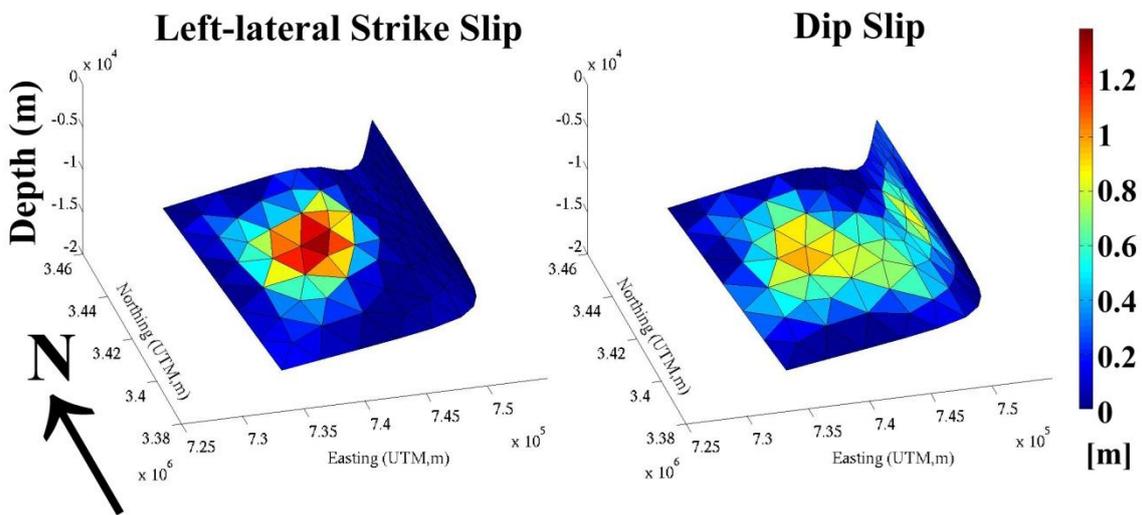
Figure 3.5 the strike slip and dip slip

3.1.5 Conclusion

Many seismologists have done lots of research about these earthquakes due to the complex topography of Tibetan Plateau, earthquake often happened there. J.R. Elliot et al. have studied five normal earthquakes occurred during 2008 in Tibetan plateau, and in which also included the Mw 6.7 Aug. 25th Zhongba earthquake. They choose to model

the earthquake as having occurred on two separate fault segments, and by their research, they found the slip was between depth of 3 and 20 km and maximum slip was about 1.2 m.

We used InSAR technology to measure the earthquake happened on Aug. 25th 2008. Both ALOS/PALSAR and Envisat/ASAR data which we used gave us a clearly inference pattern. Using Gmsh and Matlab, we made a three dimension model to detect the slip distribution, and ~1.2 m strike slip and ~0.9 m dip slip was found by our research.

Compared with the information given by GCMT, the calculated moment magnitude had an agreement with the GCMT. While, the location is about 28km away from the location given by GCMT, and the depth is about 10km shallower than the information given by GCMT.

3.2 December 20th 2010, Iran (Mw6.5) and January 27th 2011, Iran (Mw6.2)

3.2.1 Background

Iran is located in the boundary region of Arabian and Eurasian plates, and the active tectonics of Iran is basically controlled by the collision of the two continental plates with a convergence rate of ~25 mm/yr. About half of the shortening is accommodated to the Zagros range, and the latter half has been accommodated to several north-south trending right-lateral strike slip faults that surround the Dasht-e Lut desert. Little is known, however, about contemporary deformation around the Lut desert and areas further to the east, although there occurred historically a number of inland earthquakes.

On December 20, 2010 and January 27, 2011, there occurred two moderate-sized earthquakes inside the Lut "block". Our purpose to study these earthquakes is to better understand the rupture processes of intra-plate earthquake, using co-seismic deformation data from Synthetic Aperture Radar (SAR). While intra-plate earthquakes are often smaller than those occurred at major plate boundaries, they could be even more disastrous to local residents, and they also play an important role to accommodate regional tectonic stresses from the nearby plates.

3.2.2 20th Dec. 2010 Mw6.5 earthquake

3.2.2.1 Observed area and Dataset
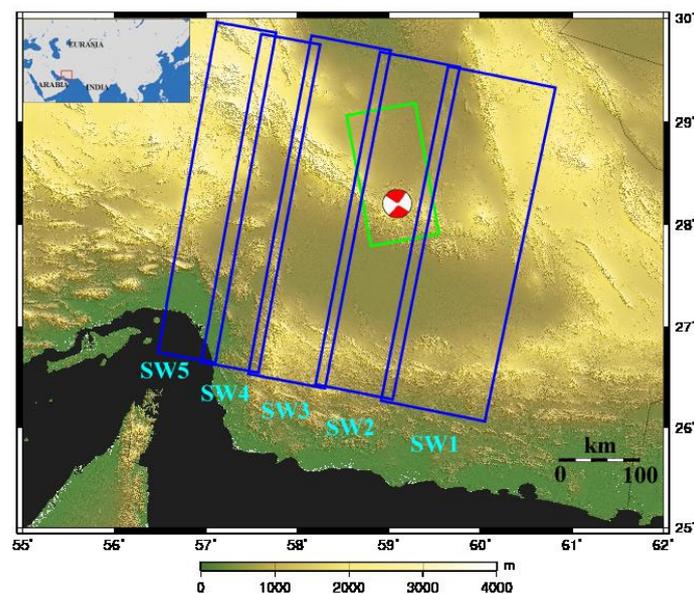
Figure 3.6 the region we used.

Table 3.2 The data table

Pair No.	Master (yyyy/mm/dd)	Slave (yyyy/mm/dd)	Bperp[*] (m)	Span (days)	Orbit	Mode
1	2010/09/30	2010/12/31	179	92	Ascending	Strimp
2	2010/07/13	2011/01/13	1124	184	Decending	ScanSAR

3.2.2.2 Interference Pattern and Pixel Offset

As InSAR (Interferometric Synthetic Aperture Radar) technology is useful for mapping the deformation of the earth's surface caused by earthquake, we processed one ascending stripmap-mode pair and one descending pair of ScanSAR data both from ALOS (Advanced Land Observation Satellite) to detect the deformation caused by this earthquake. Deformation fringes could be clearly seen by both stripmap-mode SAR data and ScanSAR data. For ascending SAR data, the maximum LOS (Line Of Sight) displacement is ~25 cm away from satellite, while the LOS displacement for ScanSAR data is ~15 cm away from satellite.
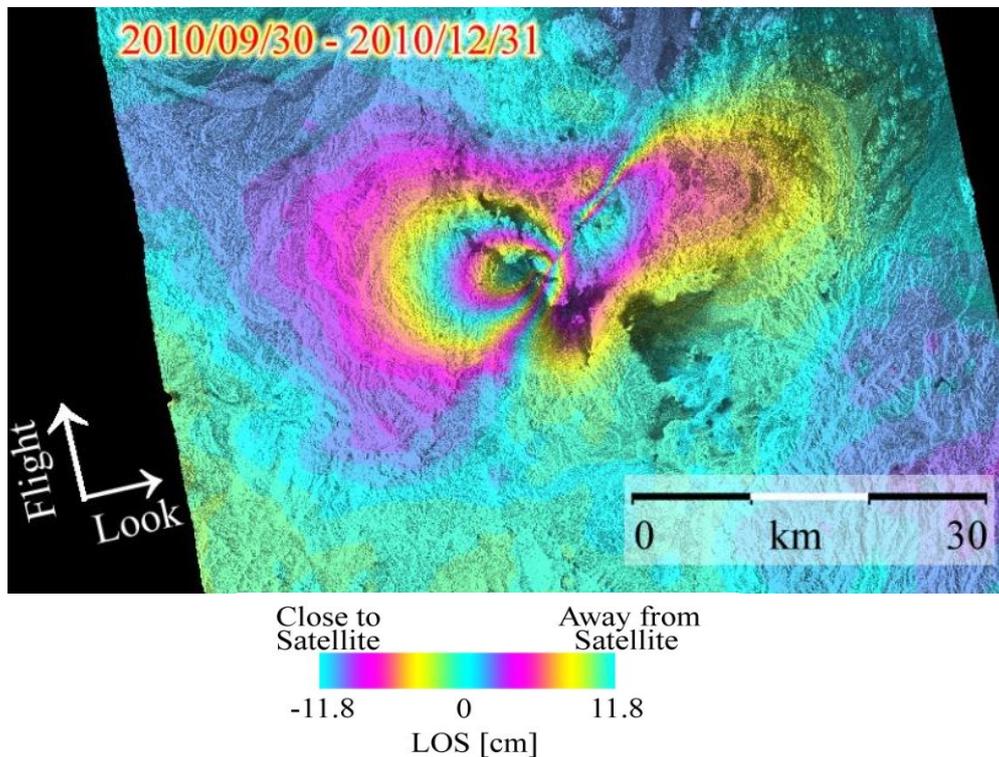
Figure 3.7 the interferogram of stripmap-mode

2010/07/13 – 2011/01/13

Look
Flight

0   km   30

Close to Satellite   Away from Satellite

-11.8   0   11.8
LOS [cm]
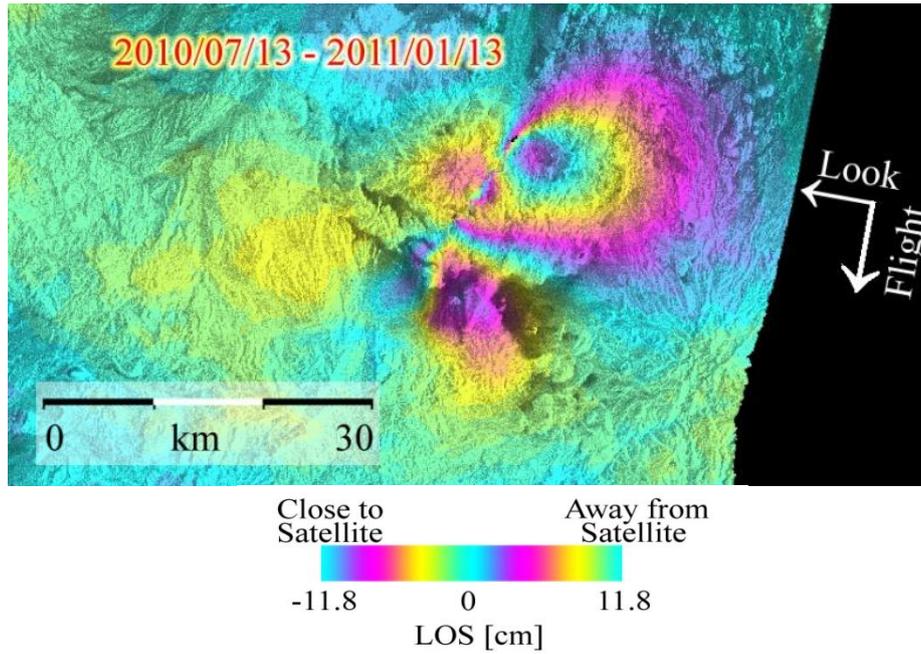
Figure 3.8 the interferogram of ScanSAR mode

2010/09/30 – 2010/12/31

Flight
Look

0   km   30

-0.25m   0.25m
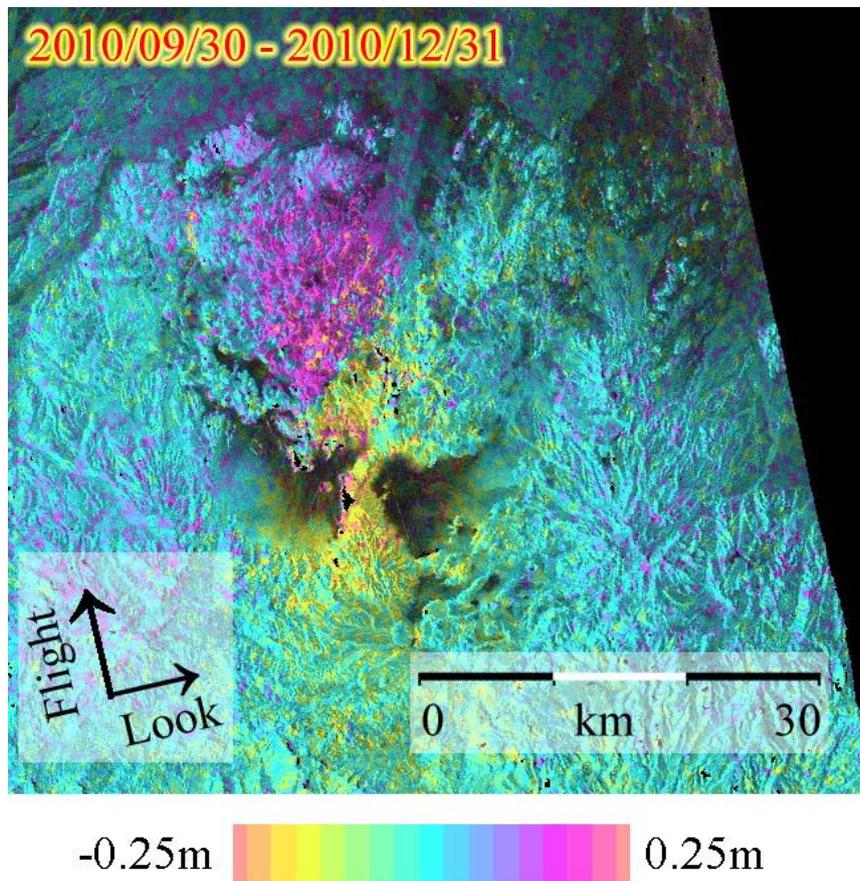
Figure 3.9 the Pixel offset data

3.2.2.3 Inversion Results

We made a fault source model to account for the observed co-seismic deformation. Our best-fitting model tells that the strike and dip angle are ~N50°E and ~84°, respectively, both of which agree with the result from Global CMT (Centroid-Moment-Tensor). The maximum slip is ~2 m and occurred at a depth from 4 to 8 km from the surface. The moment magnitude calculated by our best-fitting model is 6.5, which is also in a good agreement with the magnitude given by Global CMT.
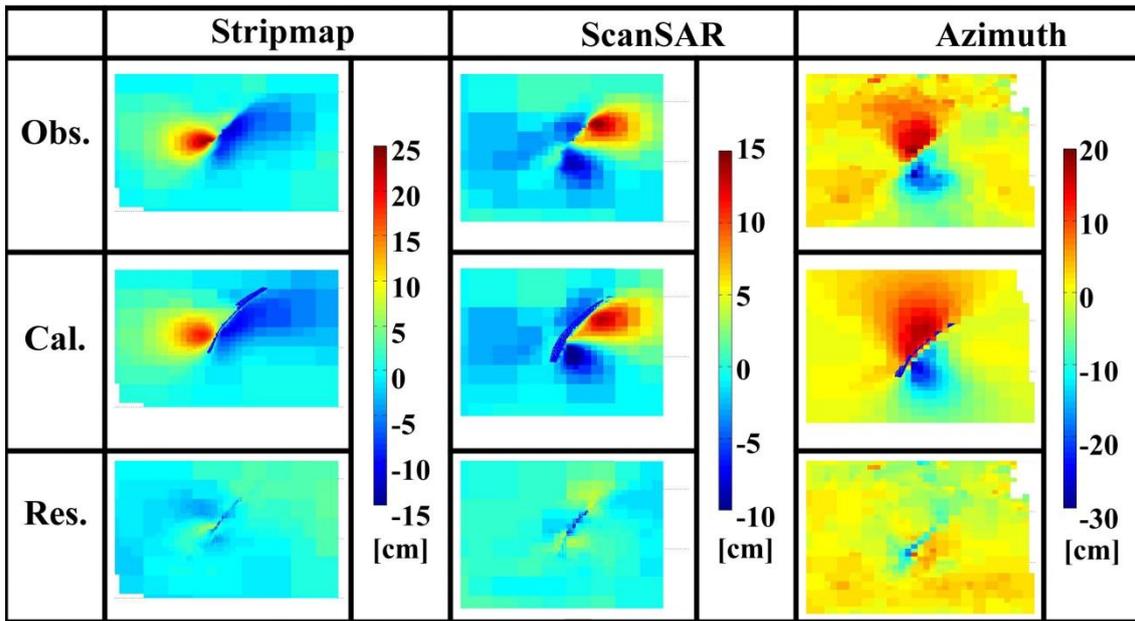
Figure 3.10 the inversion result
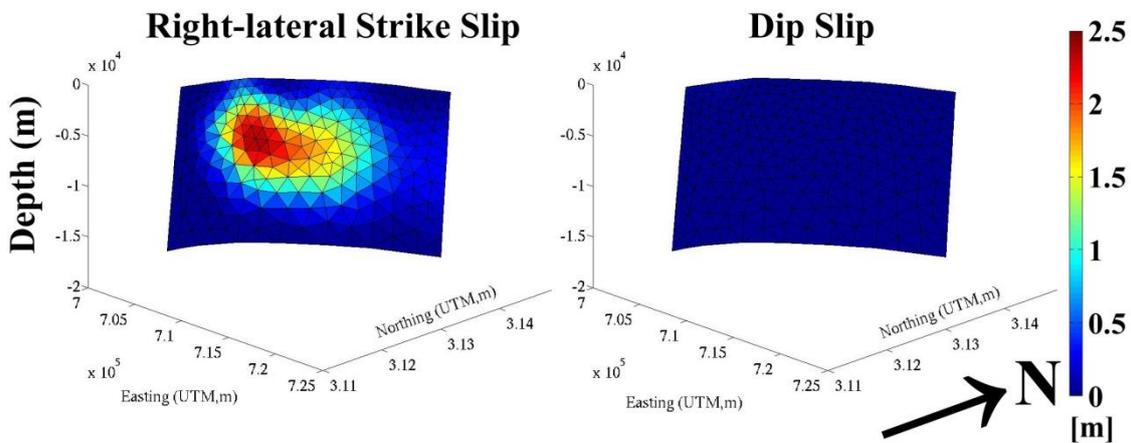
Figure 3.11 strike slip and dip slip

3.2.3 27th Jan. 2011 Mw6.2 earthquake

3.2.3.1 Observed area and Dataset
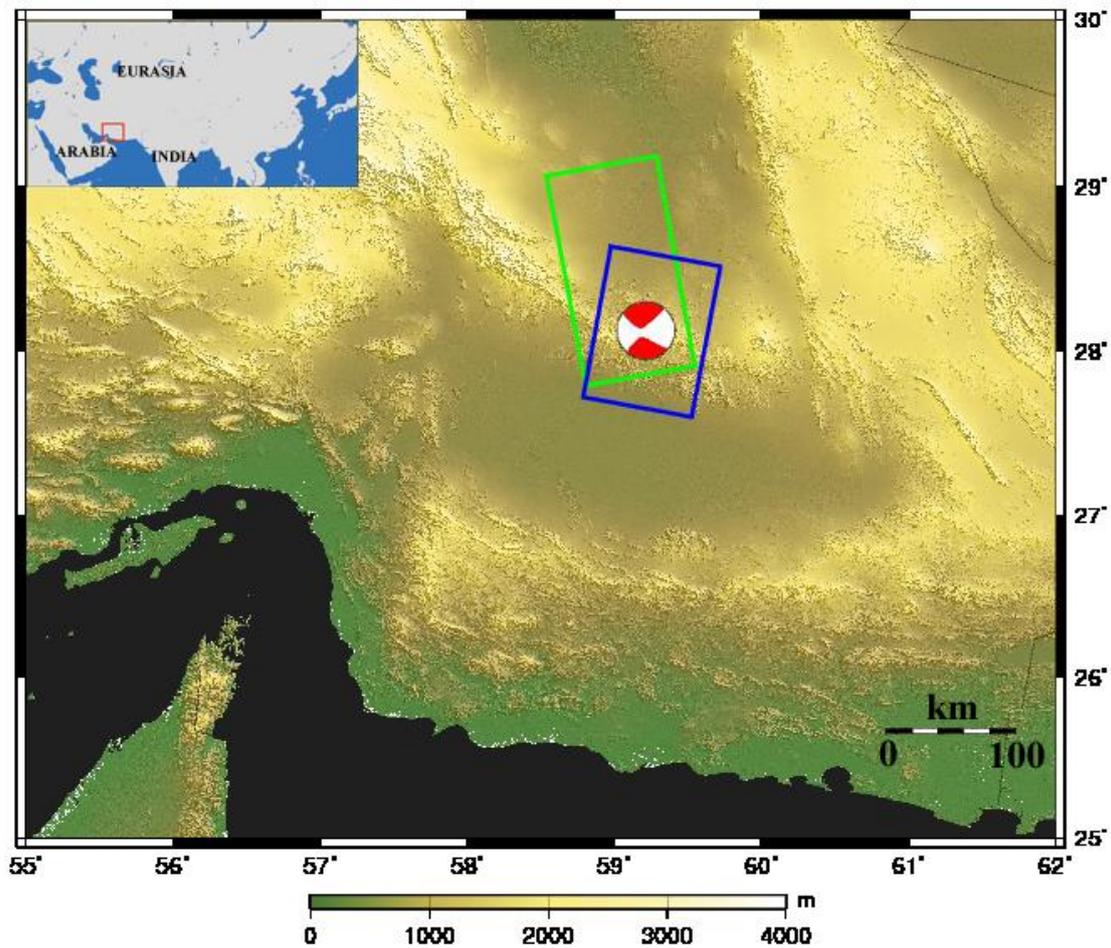
Figure 3.12 area of the research

Table 3.3 The data table

Pair No.	Master (yyyy/mm/dd)	Slave (yyyy/mm/dd)	Bperp* (m)	Span (days)	Orbit	Satellite
1	2010/12/31	2011/02/15	515	46	Ascending	ALOS
2	2011/01/25	2011/02/24	-241	30	Decending	Envisat

3.2.3.2 Interference Pattern

Another earthquake took place on Jan. 27th 2011 with magnitude of 6.2, and the hypocenter is ~30km distant away to the SW from the December event. Thus, the January event will not be a simple aftershock, but the relationship is uncertain. Both ascending ALOS SAR data and descending Envisat data have been processed to generate the co-seismic deformation signals. The maximum LOS displacement from ascending ALOS data is ~8 cm, and the descending Envisat data gives the maximum

LOS displacement ~6 cm.
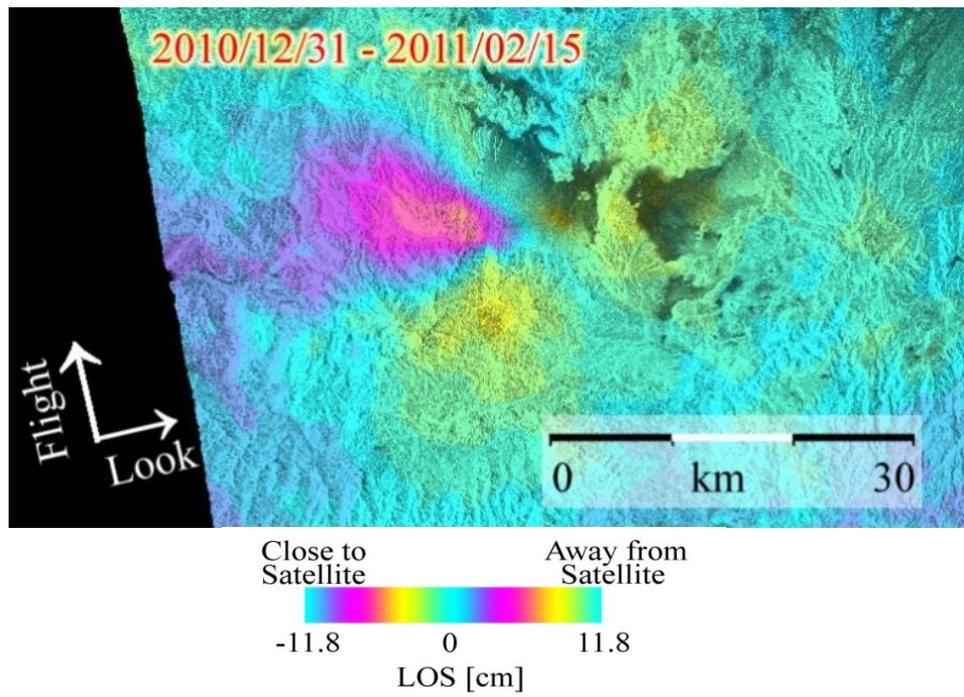
Figure 3.13 the interferogram of ALOS
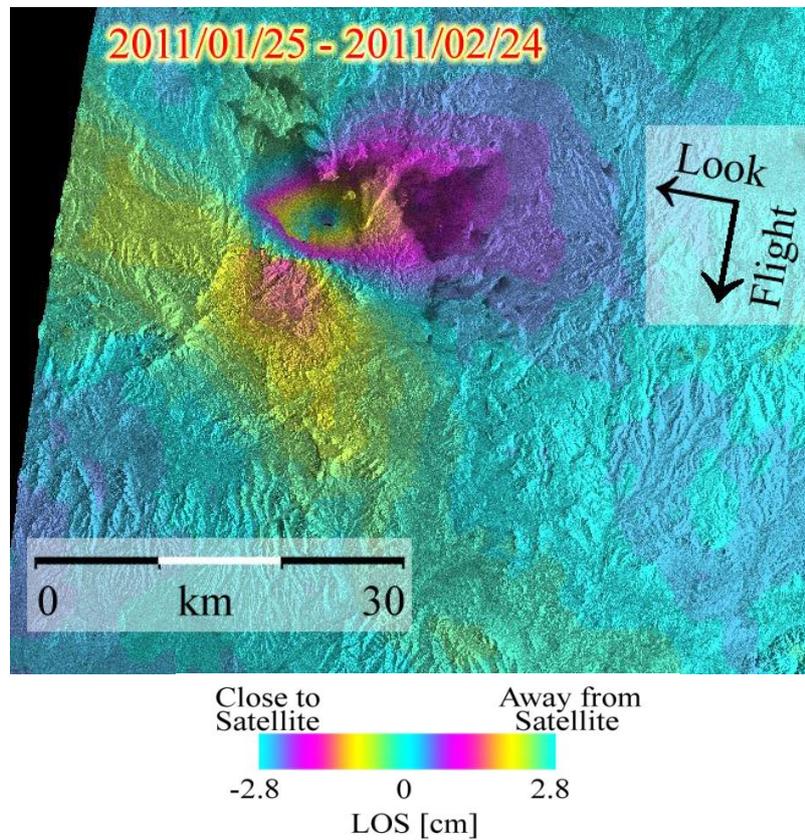
Figure 3.14 the interference pattern of Envisat

3.2.3.3 Inversion Result

Using the same method, we constructed a fault source to invert slip distribution. Our preliminary model reveals that the strike and dip angle are ~N145°E and ~85°, respectively, both of which are in agreement with the data from Global CMT. The maximum slip amplitude was ~1 m, and occurred at a depth of ~8 km.
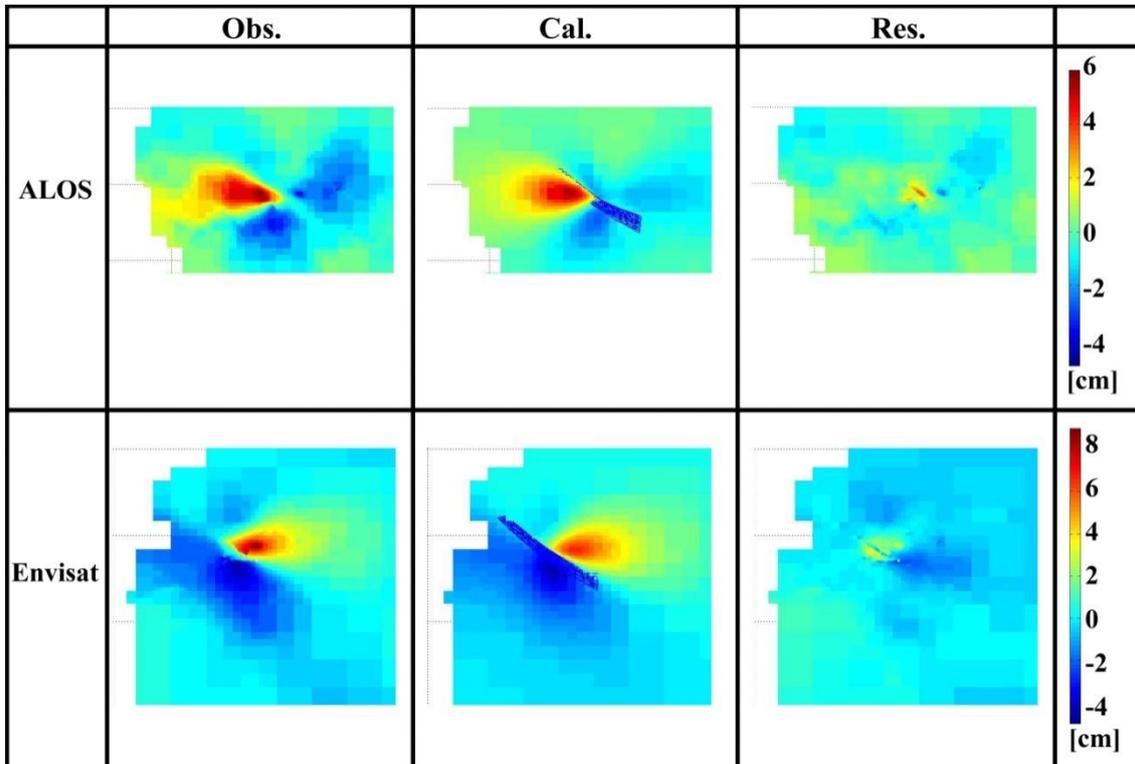

Figure 3.15 the result of inversion using three independent data, strimp-mode SAR data and ScanSAR mode data, also the Pixel offset data.
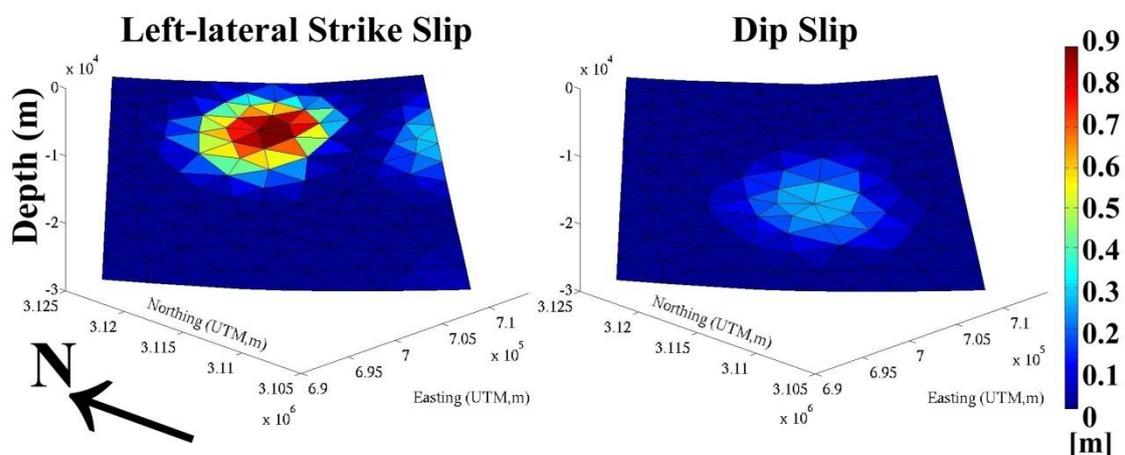

Figure 3.16 the strike slip and dip slip

3.2.4 Conclusion

Although there are no geologically mapped major faults in SE Iran, both historical and our studied inland earthquakes indicate that SE Iran is actively deforming presumably due to the collision of the Arabian and Eurasian plate. Our fault modeling indicates that the strike direction of two earthquakes is nearly perpendicular. This result suggests that the shortening between the Arabian and Eurasia plate may be accommodated along conjugate strike slip fault systems in the eastern Iran. Very few thrust faulting earthquakes take place over the area, which seems similar to the middle to northern Tibetan plateau.

For both of the two recent SE Iran earthquakes, the calculated moment magnitude had a good agreement with the GCMT. While there still some difference, for the Dec. earthquake, the location is about 12km away from the location given by GCMT and the depth is 9km shallower than the information given by GCMT; for the Jan. earthquake, the location is about 14.8km away from the location given by GCMT, and the depth is about 10km shallower than the information given by GCMT.
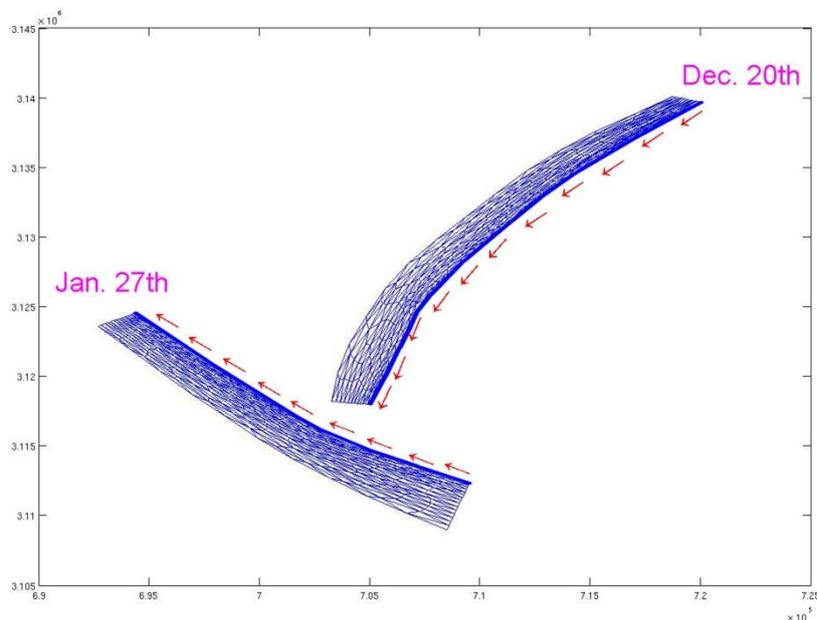

Figure 3.17 the location of two models

From our best-fitting model, the two recent earthquakes did not happen in a single fault plan, and this kind of data cannot be known by GCMT.

4. Summary

We explained the basic methods we usually used to process the SAR data, and the procedure of InSAR and Fault Source Modelling. Since InSAR data is not sensitive to the displacement in the south and north direction, we also explained Pixel Offset which can detect the displacement in azimuth and range direction.

We observed co-seismic crustal deformation of the Aug. 25th, 2008 Zhongba earthquake and the two recent earthquakes happened in SE Iran. Both ALOS/PALSAR and Envisat/ASAR data have been used, and each of the interferogram can be clearly seen.

We generated fault source models of the three earthquakes using two or three interferograms, and each calculated moment magnitude is in a good agreement with GCMT. While each depth give by our best-fitting model is about 8~10km shallower than the information given by GCMT, in addition, the location is about 10~30km away from the location given by GCMT. The two recent SE Iran earthquakes did not happen in a single fault plane by our best-fitting model, and this kind of information cannot be known by GCMT.

5. Acknowledgement

6. References

Massonnet, D., and Feigl, K. L., 1998. Radar interferometry and its application to changes in the earth's surface, Rev. Geophys., 36: 331.

Massonnet, D., Rossi, M., Carmona, C., Adragna, F., Peltzer, G., Feigl, K., and Raboute, T., 1993. The displacement field of the Landers earthquake mapped by radar interferometry. Nature, 364: 138.

Michel, R., Avouac, J.-P., and Taboury, J., 1999. Measuring ground displacements from SAR amplitude images: Application to the Landers earthquake, Geophys. Res. Lett., 26:875.

Tobita, M., Murakami, M., Nakagawa, H., Yarai, H., and Fujiwara, S., 2001a. Two-dimensional field of Three-dimensional Components of Deformations and Velocities, and Volume Change around Usu Volcano Associated with the 2000 Eruption by Matching of SAR images (in Japanese), J. Geogr. Surv. Inst., 95: 37.

Fialko, Y., Simons, M., and Agnew, D., 2001. The complete (3-D) surface displacement field in the epicentral area of the 1999 Mw7.1 Hector Mine earthquake, California, from space geodetic observations, Geophys. Res. Lett., 28: 3063.

Tobita, M., Murakami, M., Nakagawa, H., Yarai, H., Fujiwara, S., and Rosen, P. A., 2001b. 3‑D surface deformation of the 2000 Usu Eruption measured by matching of SAR images, Geophys. Res. Lett., 28: 4291.

Hanssen, R. F., 2001. Radar Interferometry: data interpretation and error analysis, Kluwer Academic Publishers, Dordrecht.

Kobayashi, T., Takada, Y., Furuya, M., and Murakami, M., 2009. Location and types of ruptures involved in the 2008 Sichuan Earthquake inferred from SAR image matching, Geophys. Res. Lett., 36: L07302.

Zebker, H. A., Rosen, P. A., Goldstein, R. M., Gabriel, A., and Werner, C. L., 1994. On the derivation of coseismic displacement fields using differential radar interferometry: The Landers earthquake, J. Geophys. Res., 99(B10): 19617.

J.R. Elliott, et al. Extension on the Tibetan plateau: recent normal faulting measured by InSAR and body wave seismology. Geophysical Journal International. 2010, 183, 503-535

Meyer, B. and K. Le Dortz (2007), Strike‑slip kinematics in Central and Eastern Iran: Estimating fault slip‑rates averaged over the Holocene , Tectonics , 26 , TC5009, doi:10.1029/2006TC002073.

Walker, R. T., et al. (2010), Active faulting, earthquakes, and restraining bend development near Kerman city in southeastern Iran, J. Struct. Geol., 32 (2010) 1046-1060, doi:10.1016/j.jsg.2010.06.012.

http://en.wikipedia.org/wiki/Advanced_Land_Observation_Satellite

http://www.eorc.jaxa.jp/ALOS/en/index.htm

http://vldb.gsi.go.jp/sokuchi/sar/mechanism/mechanism05-e.html

http://en.wikipedia.org/wiki/Envisat

https://earth.esa.int/web/guest/missions/esa-operational-eo-missions/envisat